Eur. Phys. J. B **46**, 367–376 (2005)
DOI: 10.1140/epjb/e2005-00266-4

THE EUROPEAN PHYSICAL JOURNAL B

# Asymmetric distribution of surface second harmonic generation for thin silver films deposited on Si(111)

C.-S. Chen[1] and J.-T. Lue[2,a]

[1] Department of Electrical Engineering, National Tsing Hua University, Hsin Chu, Taiwan
[2] Department of physics, National Tsing Hua University, Hsin Chu, Taiwan

Received 24 January 2005
Published online 18 August 2005 – 

**Abstract.** The asymmetric distributions of surface optical second harmonic generation (SHG) through azimuthally angular scans of (111) silicon wafers on which thin silver films were deposited, have been detected with different polarizations of output beams. On account of the inversion symmetry of silicon crystals, the SHG for the Ag/Si system is mainly contributed by the silver film and the silicon surface. In this work, we found that the interface strain implies an asymmetric intensity variation of SHG with respect to the surface azimuthal angles as an ultra thin Ag film is deposited on silicon wafers. This asymmetric behavior is prominent as the deposited silver layer is heated so that the continuous film aggregates to become granular nanoparticles. Similar changes of the surface asymmetric SHG are observed for a bare Si wafer imposed upon by an external force.

**PACS.** 78.67.Bf Nanocrystals and nanoparticles – 42.65.Ky Frequency conversion; harmonic generation, including higher-order harmonic generation – 61.25.Mv Liquid metals and alloys

## 1 Introduction

Surface second harmonic generation (SHG) from metals was established on the existence of the nonlinear $E(\nabla \cdot E)$ source term, where $\nabla \cdot E$ is the gradient of the electric field, which has a large contribution at the boundary due to the discontinuity of the lattice structure; and the presence of the bulk magnetic dipole term $E \times \partial H/\partial \mathrm{t}$ arising from the Lorentz force of electrons. Up to now, many stimulated theoretical and experimental SHG studies of bulk metals have been developed [1–6] and are continually attracting much attention. Accordingly the theory of SHG from metal surfaces was built up and modified by the phenomenological parameters $(a, b)$ which, respectively, express the components of current density that are normal and parallel to the surface as proposed by Rudnick and Stern [5]. However, the discussion of azimuthally scanned SHG depending on the interface relation of metal films and the formation of nanoparticles on silicon substrate is still rarely reported [7].

As far as the SH field of centrosymmetric material such as Si(111) substrate is concerned, the bulk contribution of electric dipoles is zero, and the lowest order nonlinear polarization density is embodied in bulk magnetic dipoles and electric quadrupoles. The surface contribution comes from the underneath term within the Thomas-Fermi screen length arising from the breaking of the lattice periodicity and the existence of dangling bonds caused by desorbed molecules. Sipe et al. [8] and Heinz et al. [9] have discussed the phenomenology of bulk and interface SHG from cubic centro-symmetric crystals in detail, which was verified by experiment. Concerning the dominated contributions of SH intensity on metal surfaces, three nonlinear sources originate from (1) the bulk current within the penetration depth embodied in magnetic dipoles and quadrupoles, and (2) two surface current sources within the selvedge region which are, respectively, parallel and normal to the metal-vacuum interface. When a thin sliver film is deposited on silicon substrates, on additional SH field arises from the anharmonic oscillation induced by the strain existing in the interlayer. Consequently the symmetric pattern of the azimuthal SH intensity, contributed to by the zincblende silicon surface, will be distorted by the non-uniform interface strain.

Previously we have derived formulae for evaluating the SHG from thin metallic films [10,11] and found that SH waves are essentially generated from the electric quadrupole of the bulk and dipole sheets within the selvedge region. The nonlinear optical reflectivity of $SiO_2/Ag/SiO_2/Ag/SiO_2$ multilayer structure was evaluated to characterize the interface structures [12,13]. Later, we employed the hydrodynamic theory and observed the dependence of incident-angles on the SHG intensity at various thicknesses of silver films deposited on glass substrates [7]. Also, the interface strains inherited by

[a] e-mail: jtlue@phys.nthu.edu.tw

the molecular-beam-epitaxially (MBE) grown III–V compound films on silicon substrates were diagnosed by analyzing the $\psi$-scan of surface SHG patterns [14].

In this work we measured the surface $\psi$-scan of the SHG pattern for thin silver films and nanoparticles on Si(111) substrates. The Ag nanoparticles were obtained by rapid thermal annealing of a thin Ag film coated Si substrates. The particle sizes are strongly related to the thickness of deposited thin films. The nonlinear optical susceptibility is attributed to polycrystalline Ag nanoparticles in ellipsoidal shapes [15]. For an Ag/Si system with a film thickness less than the penetration depth, the SH nonlinear susceptibility is due to many factors such as the difference in normal polarizations between the top and bottom sides, the electron-plasmon oscillation, the field enhancement due to non-spherical shape, and the possible dipole field arising from the breaking of inversion symmetry induced by interface-strain. A weaker SH intensity of the annealed Ag/Si film than that of the virgin film results from the small filling factor of the aggregated nanoparticles and their spherical shape. The non-uniform interface strain relaxes during the thermal annealing process resulting in the $3m$-symmetry behavior of the condensed nanoparticles. In addition, we introduced the SH intensity patterns of an artificially imposed force on Si(111) substrates to adduce the evidence of the asymmetric distribution of surface SHG induced by interlayer strain.

## 2 Theory

For centro-symmetric media such as silicon substrates, the remnant electric dipoles that contribute to the SHG are the surface terms within a selvedge region of several angstroms such as

$$P_{iS}^{2\omega} = \chi_{S,ijk}^{(2)} : E_j(\omega) E_k(\omega), \tag{1}$$

where $\chi_{S,ijk}^{(2)}$ is the second-order susceptibility tensor relevant to the surface symmetry structure and electric polarization of the surface layer arising from dangling bonds and adsorbed molecule. Below the selvedge region, but within the penetration depth, the bulk terms receive contributions from electric quadruples and magnetic dipoles that yield the $i$th component of the nonlinear bulk polarization as given, respectively, by [16]

$$\begin{aligned} P_{b,i}^{2\omega} &= \gamma\nabla_i(\vec{E}.\vec{E}) + \varsigma(\vec{E}_{\times}\vec{\nabla}\times\vec{E})_i \\ &= \gamma\nabla_i(\vec{E}.\vec{E}) + \varsigma\frac{j\omega}{c}(\vec{E}_{\times}\vec{H})_i \end{aligned} \tag{2}$$

where $\gamma$ and $\zeta$ are non-zero isotropic and anisotropic parameters, respectively. The first term represents a gradient vector that is independent of the orientation of principal crystallographic axes, and the second term shows an anisotropic contribution relating to the crystal symmetry depending on the azimuthal angle $\varphi$. For either the p- or s-polarized fundamental radiation, the phenomenological theory given by Sipe et al. [8] delineates the variation of the SH field on azimuthal angles for the Si(111) crystal surface with $3m$-symmetry as given by

$$E_p^{2\omega} = a_p(\theta) + c_p\cos(3\varphi), \tag{3a}$$

$$E_s^{2\omega} = b_s\sin(3\varphi), \tag{3b}$$

where $a_p$ , $b_s$, and $c_p$ are linear combinations of the surface and bulk nonlinear susceptibilities including the combination of isotropic constant $\gamma$ and the non-vanished susceptibility tensor elements. For the coefficient $a_p = 0$, which is a function of the incident angle $\theta$, the generated scan of the surface SH is a symmetric six-fold pattern and for $a_p \neq 0$, an asymmetric six-fold lobe is observed. For a thin silver film deposited on a Si(111) substrate, the total SH field originates separately from the above described magnetic dipole and electric quadrupole terms of the thin silver film, and the interface-strain induced nonlinear polarization.

Elastic strain is evoked near the interface resulting due to a misfit of the lattice constant of the film with the substrate. This asymmetric distribution of the second-order nonlinear optical susceptibility induced by the strained layers has also been found in other systems [16,17]. The misfit factor can be expressed as $f = (a_f - a_s) / a_s$, where $a_s$ and $a_f$ are the lattice constants of the substrate and film, respectively. In equation (2), the interface strain not only contributes to the extra nonlinear polarization to the isotropic term $\gamma$ but also enhances the anisotropic term $\zeta$ due to the increased thickness of silver films [18]. Goverkov [19] expressed the azimuthally angular dependence on the p-polarized SHG for a p-wave incident beam by

$$I_{P-P} \sim [\chi_{xxx}^{(2)IH}\cos 3\varphi + \delta]^2, \tag{4}$$

where $\chi_{xxx}^{(2)IH}$ means the inhomogeneous strain induced contribution to the nonlinear optics (NLO) susceptibility, and $\delta$ is a linear combination of the $\chi_{ijk}^{(2)IH}$ elements. Accordingly, the isotropic and an-isotropic terms in equation (4) increase with the inhomogeneous strain. In reference [16], the non-vanished elements of the second-order NLO susceptibility of the Si(111) strained lattice have been demonstrated. In addition, the surfaces of thin metal film excited by external irradiation can generate the second-order nonlinear optical response that consists of a "surface" current density penetrating only a few Thomas-Fermi screening lengths below the metal surface (the so-called selvedge region) and a "volume" current density that extends over the skin-depth. Theoretically, the "bulk" contribution depends on the thickness of the film, as the thickness is less than the skin depth. The "surface" contribution is less affected by the film thickness. In principle, the two parts of SH contributions are based on a free-electron gas or hydrodynamic model so that we can speculate that the SHG depending on the azimuth-angle yields the isotropic term $\gamma$.

We tacitly assumed that the crystalline structure of silver nanoparticles is the same as that of the original metal film. In our previous work [20] we had predicted that the magnitude of the quadrupole susceptibility is

inversely proportional to the particle size attributed to the quantum size effect as the particle size diminishes smaller than 10 nm. Aussenegg et al. [17] published a practical consideration of SHG arising from nanoparticles by assuming that a simple model of a real island film is a collection of rotational ellipsoids resting on the substrate with their long axis parallel to the surface. On account of the shape and size effect, different polarized input beams can excite different intensities of SH light. Considering that the s-polarized incident field is unable to drive the surface electron-plasmon oscillations, only the "bulk" contribution needs to be concerned. This is because the surface dipole susceptibility for each dipole is compensated by its opposite dipole when illuminated by a uniform light. However the field for the p-polarized input beam can be divided into parallel and normal components to the substrate surface. The normal component not only drives the electron-plasmon oscillation along the short axis of the oblate ellipsoid, it also excites surface dipole susceptibilities arising from the top and bottom interfaces of silver particles. All of these SH fields measured in the $\psi$-scan imply an isotropic distribution except the contribution from interface strain which yields asymmetric pattern.

To elucidate the strain induced nonlinear second-order susceptibility, we draw a schematic diagram of the interface between the thin silver films with cubic symmetry on a thick cubic silicon substrate, which is located in the $xy$-plane with the $z$-axis perpendicular to the interface as shown in Figure 1. The strain tensor in the film can be expressed as [18]

$$U_{lm}(r) = U_{lm,mis}(r)\theta(h_c - z) + U_{lm,disl}(r)\theta(z - h_c), \quad (5)$$

where $\theta(z-h_c)$ is a step function with $h_c$ being the critical thickness of the film for the demarcation of a pure lattice misfit and a mixture of the dislocation misfit. The strain tensor induced by the lattice misfit is written as

$$U_{lm,mis}(r) = f\delta_{lm}, \quad (6)$$

where $f = (a_f - a_s)/a_s$ with $a_f$ and $a_s$ being the lattice constants of the film and the substrate, respectively, and $\delta_{lm}$ being the Kronecker delta function with $l, m = x, y$. For a deposited silver film, with thickness, $d_f$, much smaller than the critical thickness $h_c$, we can neglect the strain induced by the misfit of dislocation, wherein the second-order nonlinear susceptibility can be expressed totally as

$$\chi^{(2)}_{\mathrm{ijk}}(r) = \chi^{(2,0)}_{\mathrm{ijk}}(r) + \mathrm{p_{ijklm}U_{lm}}(r), \quad (7)$$

where $\chi^{(2,0)}_{ijk}(r)$ is the original value of the free surface, and $p_{ijklm}$ is a nonlinear photoelastic tensor. For both s- and p-polarized input light, the second-harmonic radiation will be p-polarized.

## 3 Experiments

Thin silver films were deposited on Si(111) substrates in a high vacuum chamber by thermal deposition. The film thickness was monitored in situ by a quartz oscillator with the frequency-shift versus thickness calibrated by an $\alpha$-stepper. The experimental set-up for the SHG measurement is illustrated in our previous work [14]. The source of the fundamental radiation for the SH generation measurement is a passively mode-locked, Q-switched Nd:YAG laser (wavelength at 1064 nm) with a typical FWHM of 100 ps at a Q-switch repeating rate of 1 KHz. Due to the extremely narrow pulse width, the single pulse energy can be reduced to as low as 0.5 mJ to immunize from thermal radiation. The fundamental laser beam passing through a glass beam-splitter, which reflects 5% of the laser intensity on an AT-cut quartz plate, is employed as a reference SHG signal. The straight light beam on passing through a Schott glass filter illuminates the sample surface which is mounted on a computer-controlled step-motor with a focused beam spot size of $1 \sim 2$ mm$^2$, Firstly, the light reflected from the sample surface passes through a set of blocking filters, which only allows the SH wave to pass through. As depicted in Figure 1, the incident angle $\theta$ was kept at 45° during the azimuthally angular rotation (or $\varphi$-scan). A computer controlled stepping motor provides an automatic scanning of the $\psi$ angles for the sample surface orientation in every step of 0.9°. The rotation axis for the $\varphi$-scan is checked to be parallel to the incident beam as verified by observing the fixed output spot whilst rotating the silicon wafer. The precission of the orientation of the polarizer is ±0.5°.

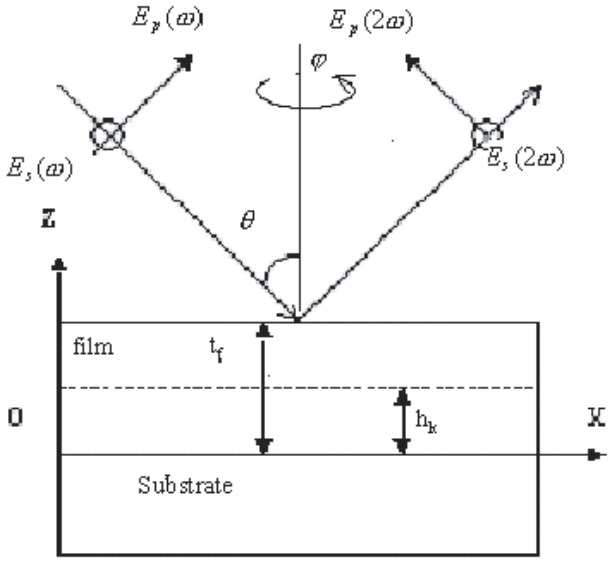


**Fig. 1.** A schematic diagram of the interface between the thin silver film, with cubic symmetry, and a thick cubic silicon substrate that is located in the $xy$ plane with the $z$-axis perpendicular to the interface.

After measuring the SHG of the silver film coated silicon wafers, the same samples were subjected to a rapid thermal annealing at 150 °C for ten minutes. Because the surface tension of Ag grains is greater than the cohesive force of Ag/Si interface, the silver film tends to aggregate to form nanoparticles as displayed in Figure 2, which were examined by a scanning electron microscope

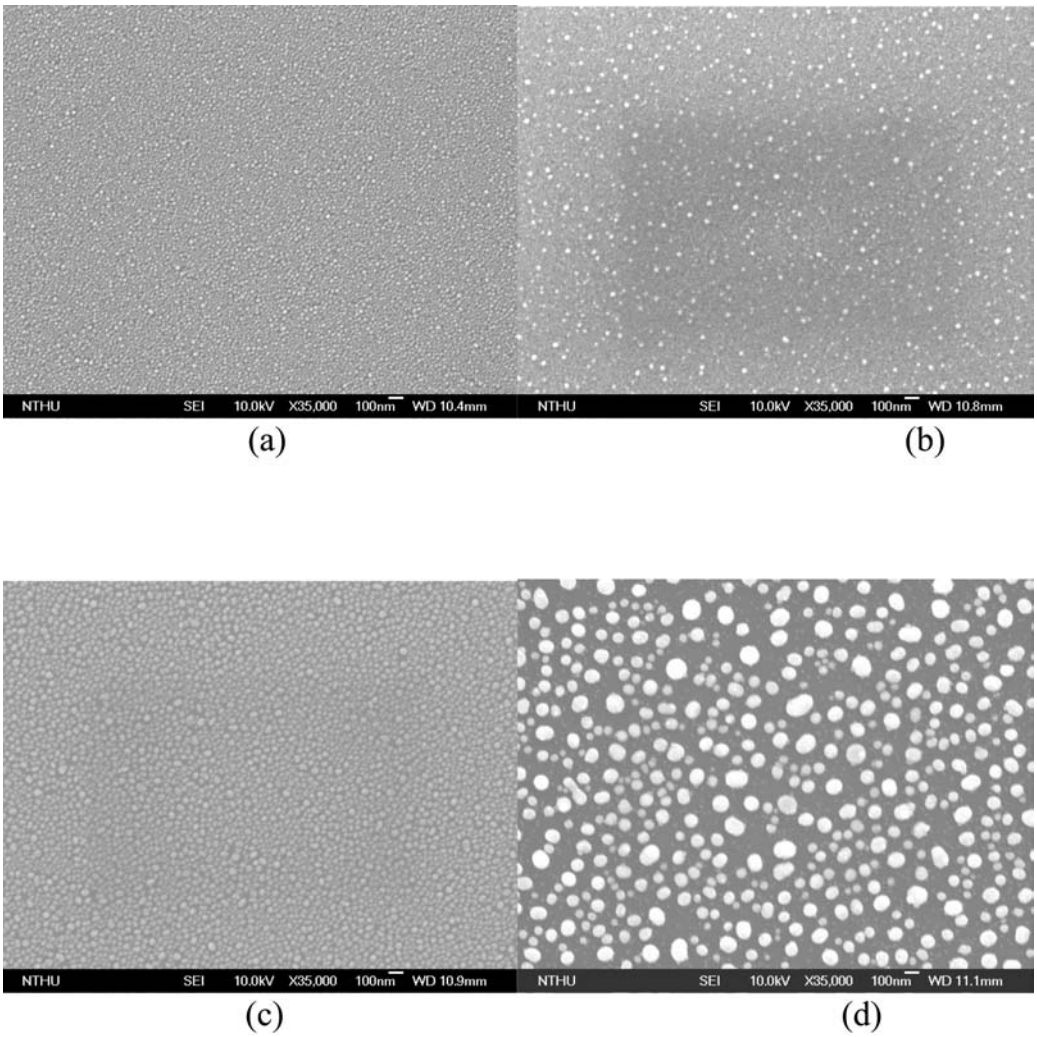


**Fig. 2.** SEM pictures of silver nanoparticles formed through a rapid thermal annealing at 150 °C for ten minutes of thin Ag films of thicknesses (a) 5 nm, (b) 9.7 nm, (c) 24 nmA, and (d) 45 nm, respectively.

(SEM). The particle size crucially depends on the film thickness, the evaporation conditions, and the annealing temperature and duration.

## 4 Results and discussions

To certify that the rotation axis of the $\psi$-scan is parallel to the incident beam, the p- and s-polarized SH fields with the fundamental p-polarized input beam for the $\psi$-scan on a clean Si(111) substrate were first measured as shown in Figures 3a and 3b, respectively. The symmetry distribution of the sixfold pattern verifies this evidence. The SHG for various thicknesses of Ag films on Si(111) substrates for the p-input and p-output are shown in Figure 4a. In all of following figures, the intensity scales are incongruent. The reduction to three-lobe distribution of the p-in and p-out occurs for the ultra-thin silver film ($\sim$5.0 nm) even the isotropic second-order nonlinear susceptibility of silver is ten times larger than that of silicon suggesting that the non-linear susceptibility due to the interface contribution inherited by the silicon substrates is enhanced by depositing silver films. The isotropic contribution of second-order nonlinear optical response for silver films progressively increases to overwhelm the anisotropic surface terms of silicon as the thickness of the sliver film increases.

Eventually, the thin silver film not only provides the isotropic contribution, but also introduces a strain at the Ag/Si(111) interface to generate an extra non-linear susceptibility to its original anisotropic susceptibility. Furthermore, increasing the silver-film thickness within the skin depth increases the isotorpic term contributed from silver resulting in a homogeneous spherical SH pattern. The lattice misfit at the interface Ag/Si(111) causes a strain that induces a strong interface dipole, which distorts the symmetric patterns of the SHG by the surface $\psi$-scan. Meanwhile the anisotropic coefficients increase with the film thickness. As the film thickness increases to 9.7 nm which is larger than the optical penetration depth of silver, the isotropic term attributed to the deposited silver is greater than that of the anisotropic term arising

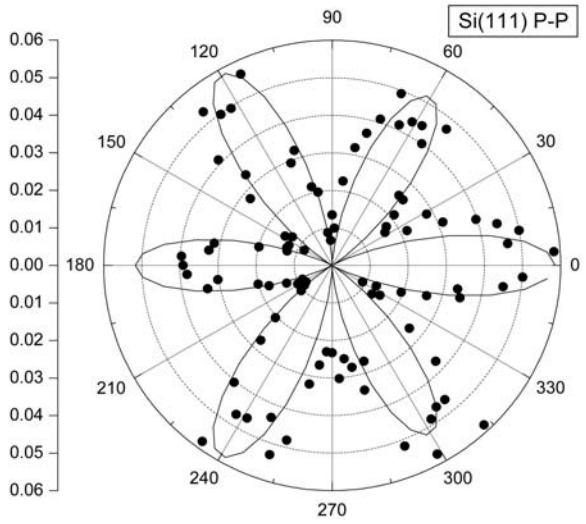


(a)

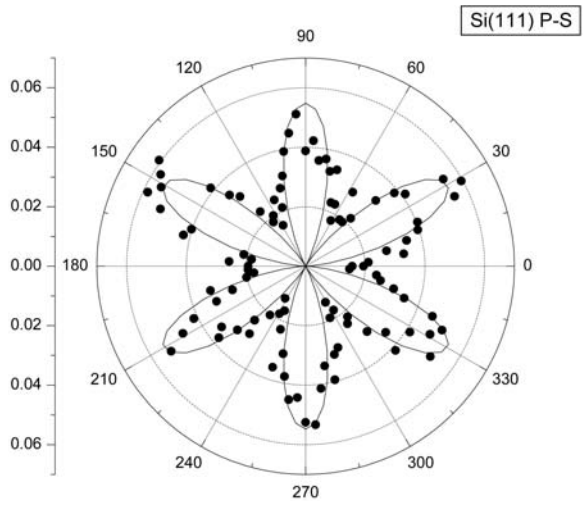


(b)

**Fig. 3.** The distribution of the $\psi$-scan for (a) the six fold asymmetric p-input and p-output, and (b) the six fold symmetric p-input and s-output, respectively for the bare Si(111) substrate.

from the interface strain of silicon surface, which results in a uniform distribution of the surface SHG by the $\psi$-scan.

For comparison, the $\psi$-scanned SHG for Ag nanoparticles aggregated from the annealed silver films are shown in Figure 4b. For ultra-thin nanoparticles (<5.0 nm), the surface scan illustrates a much distinguished threefold symmetry resulting from the enhanced non-linear anisotropic polarization induced by the Ag/Si strain below the silver islands. As the film thickness increases further the isotropic susceptibility of silver overwhelms the anisotropic terms of Si and the $\psi$-scanned SHG becomes uniformly distributed. It needs to be mentioned that nanoparticles aggregated from rapid thermal annealing (RTA) of thin silver films enhance the anisotropic surface non-linear susceptibility of Si to form a distinguished 3m symmetry of Si(111). The particle size is closely related to the original film thickness which is not in accord with the size dependence on the SH intensity as portrayed in references [19–21]. Since the thickness of an ultra thin metal film is much less than the penetration length, the total effective volume will overcome the value of quadrupole susceptibility which is inversely proportional to the nanoparticle size.

Figures 5a and 5b show the$\psi$-scan of s-polarized SH fields for the p-polarized input beam at various silver film thicknesses and grain sizes of Ag on Si(111), respectively. As illustrated in Figure 5a, only the surface isotropic and the anisotropic terms in equation (3) are enhanced by the interface strain as the silver film thickness increases owing to the lack of s-polarized SH contribution from metals. However, the non-symmetric behavior, because of strain induced nonlinear polarization as addressed in equation (6), imposes an excess contribution $g_s+\Delta P_s \sin(\Delta\psi)$ to the $\psi$-scan of the SH field pattern. The parameter $g_s$ is a constant, which represents the isotropic contribution from the interface strain. In fact, the $\psi$-scan of p-polarized SH field patterns also have a superposition factor $g_p + \Delta P_p \cos(\Delta\psi)$ on them. For simplification, we incorporate this into the factor $a_p$. The coefficient $\Delta P_{\mathrm{s(p)}}$ is the strain-induced, non-symmetric constant intrigued from the s(p)-polarized SHG. The angle $\Delta\psi$ is defined as $\psi - \psi_0$ , where$\psi_0$ depends on the strain orientation. The parameter $\Delta P_{\mathrm{s(p)}}$, dependent on the film quality and thickness, represents the degree of non-uniform inhomogeneous strain. The presence of this factor will curtail the isotropic and anisotropic contributions from the crystal structure and interface. The SH intensities from the annealed Ag/Si(111) samples are weaker than those from the virgin films as shown in Figure 5b, which results from the geometric mirror symmetry and the reduction of the effective interface area. Whereas the SH intensity increases with the size of silver particles, owing to the increase in the coverage area of the silver particles which have a higher SH susceptibility than silicon, which is attributed to metallic electron-plasmon oscillation. The threefold asymmetric pattern for the condensed island films becomes more prominent than that of the virgin films plausibly arising from the crystalline alignment of silver islands at the interface with the $3m$ symmetry of Si(111) substrates. The RTA method relaxes the nonuniform inhomogeneous strain. Table 1 lists these related fitting parameters of the SH field by different polarization geometry combinations.

To adduce the asymmetric distribution of the SHG due to the strain induced lattice mismatch of the interface layers, we measure the surface $\psi$-scan from bared silicon, using a screw to apply a micro force on the surface as shown schematically in Figure 6. The surface crystallography of atoms for the Si(111) wafer and the corresponding canted angles is shown in Figure 7. The bending direction parallel to the primary-edge flat-cut of the p-type Si(111) wafer was defined as the initial zero angle. The six fold SHG patterns are largely distorted for both the p- and s-polarized SH responses as shown in Figures 8 and 9, respectively, which also reveals that the distortion increases with the point press. The alternation from six fold

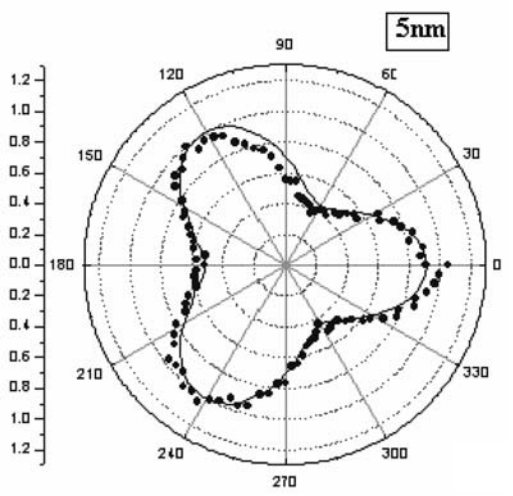


(a1)

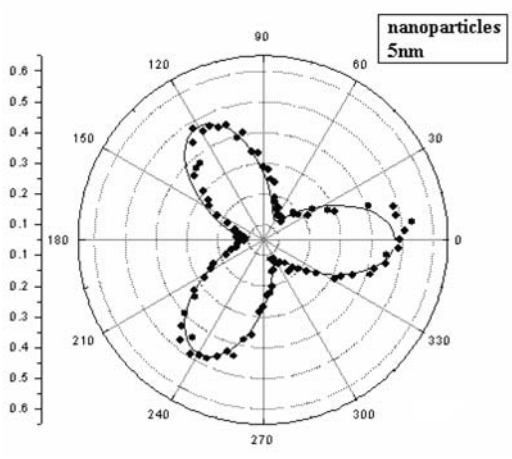


(b1)

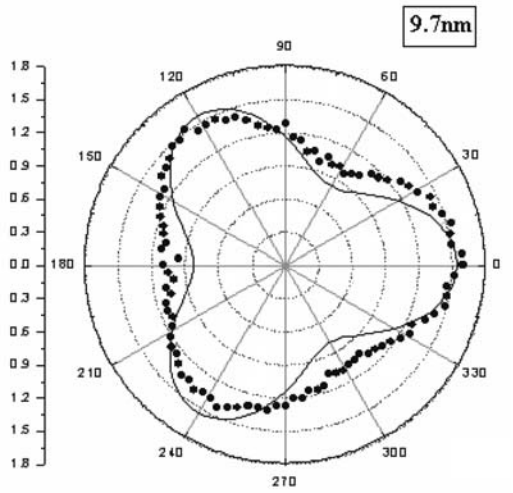


(a2)

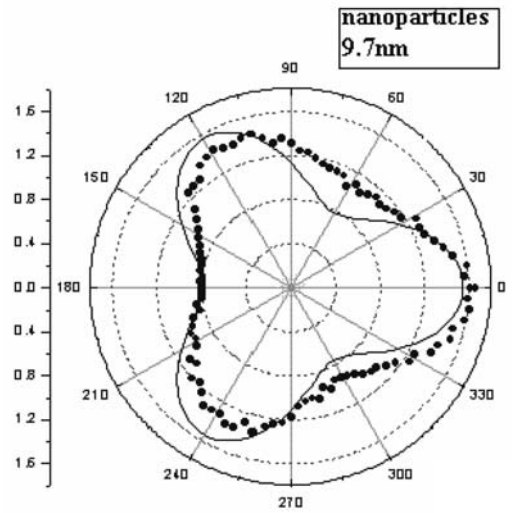


(b2)

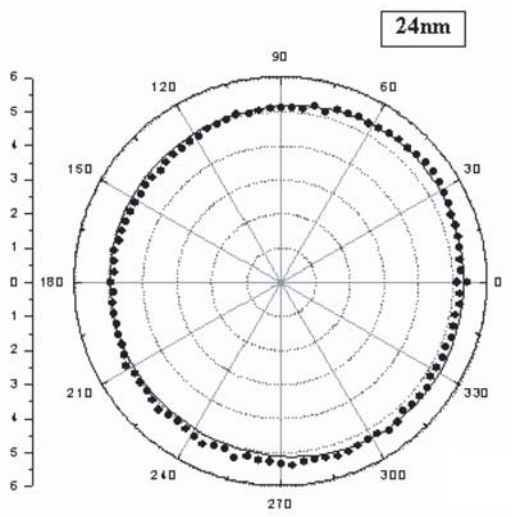


(a3)

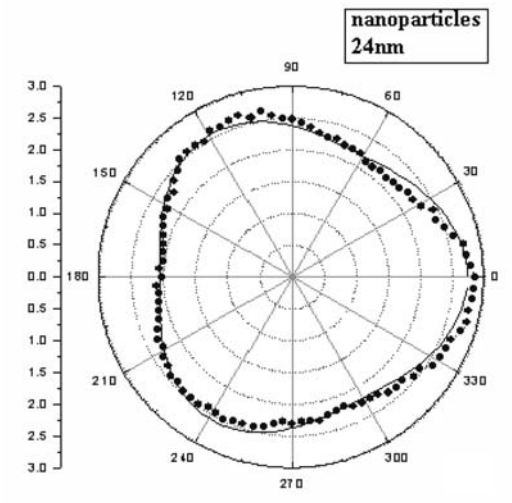


(b3)

**Fig. 4.** The $\psi$-scan of the p-polarized input and the SH p-polarized output for (a1, a2, a3) various thicknesses of silver films on Si(111) substrates, and (b1, b2, b3) various particle sizes of the nanoparticles formed by the annealing of above films.

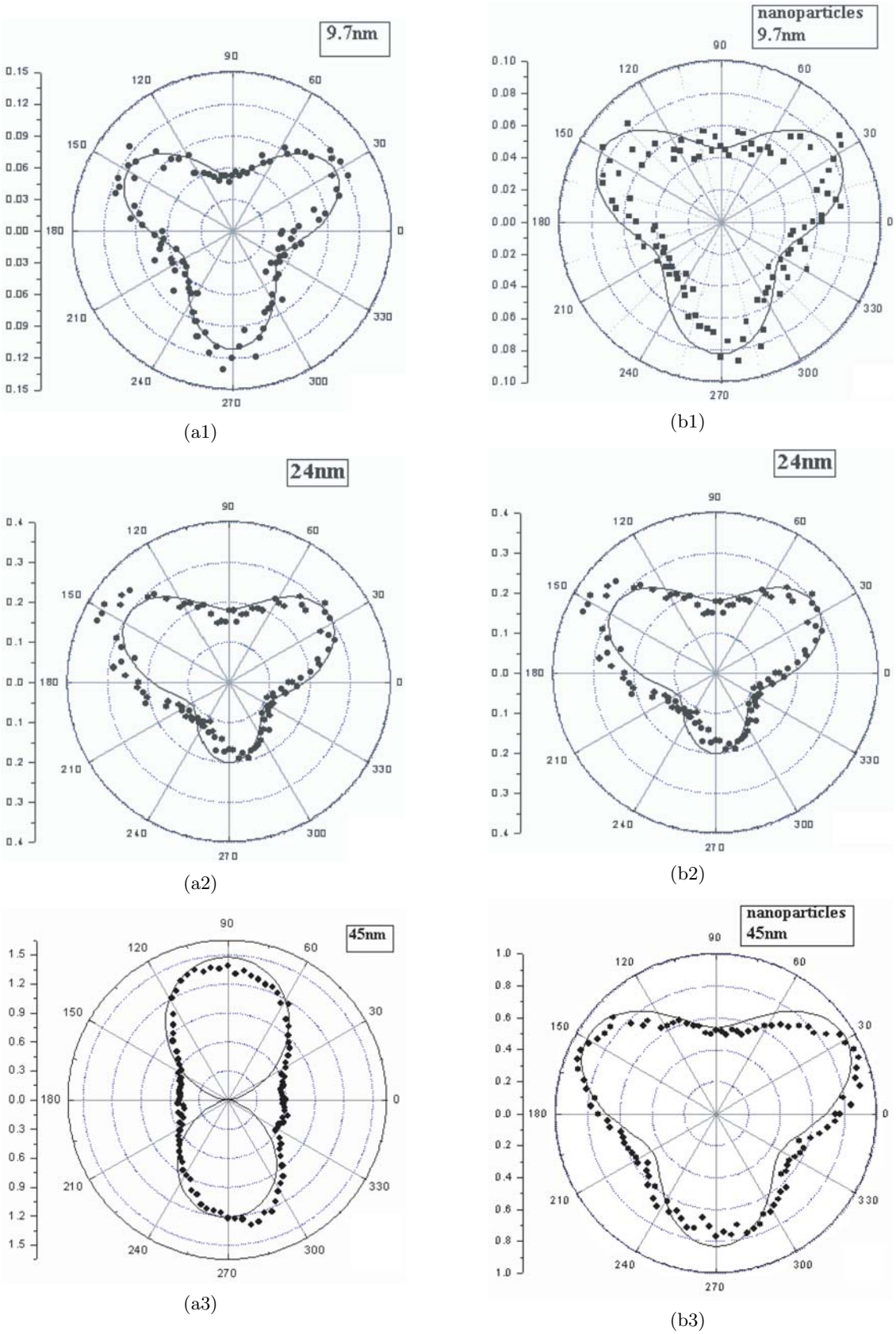


**Fig. 5.** The $\psi$-scan of the p-polarized input and the SH p-polarized output for (a1, a2, a3) various thicknesses of silver films on Si(111) substrates, and (b1, b2, b3) various particle sizes of the nanoparticles formed by the annealing of the above films.

**Table 1.** The fitting parameters for various SH fields at different polarization configurations.

| | | $a_p$ | $c_p$ | $\Delta P_p$ |
|---|---|---|---|---|
| Si(111) | | 0.024 | 0.151 | — |
| 5 nm | film | 0.837 | 0.150 | $\sim 0$ |
| | particles | 0.520 | 0.170 | $\sim 0$ |
| 9.7 nm | film | 1.074 | 0.171 | 0.000 |
| | particles | 1.061 | 0.185 | 0.000 |
| 24 nm | film | 2.268 | 0.001 | 0.050 |
| | particles | 1.542 | 0.077 | 0.041 |
| | | $g_s$ | $b_s$ | $\Delta P_s$ |
| Si(111) | | — | 0.172 | — |
| 9.7 nm | film | 0.280 | 0.055 | $\sim 0$ |
| | particles | 0.250 | 0.040 | $\sim 0$ |
| 24 nm | film | 0.436 | 0.076 | 0.063 |
| | particles | 0.258 | 0.041 | 0.018 |
| 45 nm | film | 0.055 | 0.045 | 1.227 |
| | particles | 0.842 | 0.125 | 0.035 |

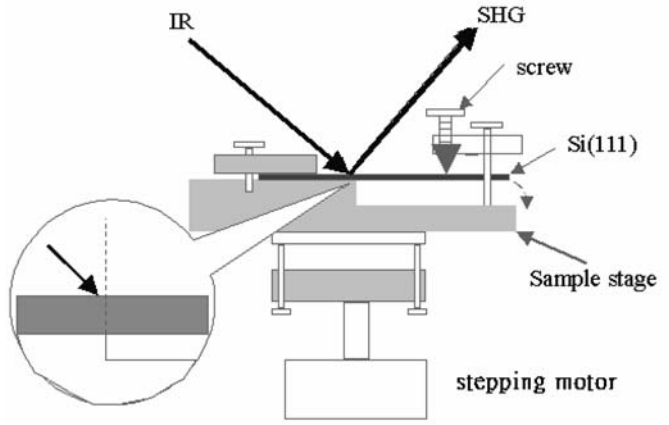


**Fig. 6.** The experimental setup for applying a micro press to a silicon wafer to induce surface strain.

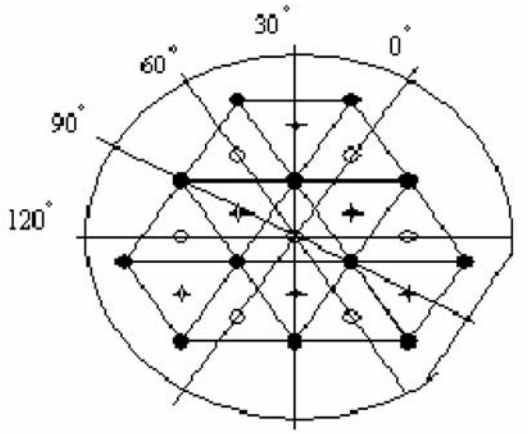


**Fig. 7.** The surface crystallography of Si atoms and orientations for the Si(111) wafer.

pattern to asymmetric two fold is clearly manifested for the s-polarized SH due to its independence of on the surface isotropic contribution $a_p$. The wafer was then rotated every thirty-degrees and we then measured the $\psi$-scanned SH intensity with three kinds of pressure imposed by the screw. To confirm the SH intensity was closely related to the azimuthal angle $\psi$, the incident angle $\theta$ was precisely calibrated. The SH intensity was measured with the fundamental input beam impinging on the bending direction.

In this experiment, we observed that the SH intensity decreases with the increase of the imposed force by the screw, implying a loss of phase coherence in the SH fields generated by the strained layers. The asymmetric SH pattern appears as the strain increases. Sophisticatedly, the anharmonic oscillating strength arising from the bulk covalent bonds changes with the bending of the wafer. This force-induced strain has a different effect on the SHG in comparison to that generated from the lattice misfit of interface layers because the latter induces interface dipoles providing excess SH contribution without destroying the bulk crystalline structure. However, the non-uniform stress provides an evidence of a strain induced asymmetric SH field distribution for the surface $\psi$-scan of the SHG pattern for thin silver films and nanoparticles on Si(111) substrates.

## 5 Conclusions

In this work we found that the threefold symmetric SH patterns of Si(111) are distorted by deposition of silver films. The nonlinear surface polarization inherited by the Ag/Si interface is enhanced for the deposition of an ultra thin layer of silver films resulting in the distinguishable three lobes of the SH pattern. The same results are found for the Ag/Si surfaces distributed with silver nanoparticles, while the three-fold pattern remains even the particle size increases to percolated islands. A strain layer existing in the interface induces additional anharmonic oscillation strength along a special crystal orientation, which results

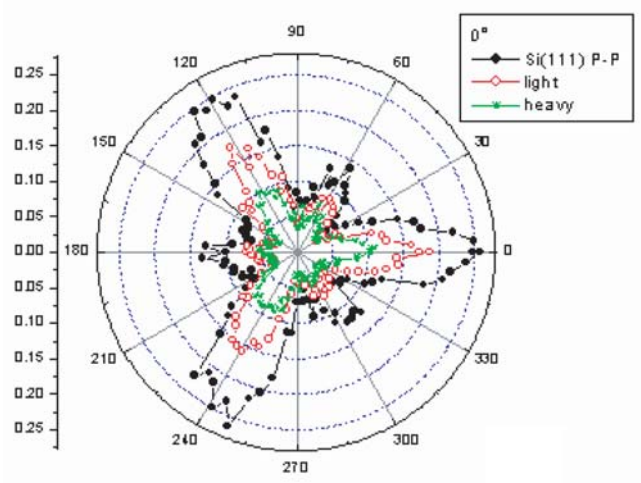


(a)

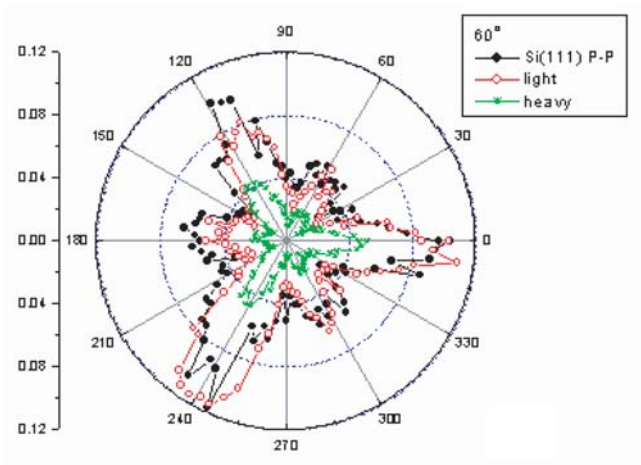


(b)

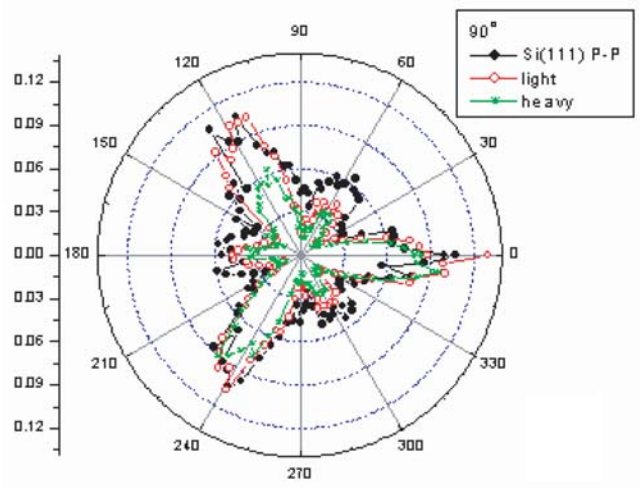


(c)

**Fig. 8.** The p-wave input and p-wave output SHG for a bare Si(111) with various imposed forces and incident azimuthal angles as indicated in Figure 7.

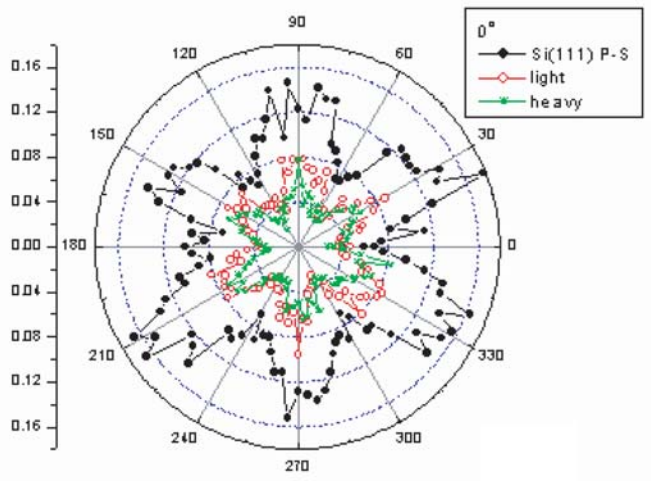


(a)

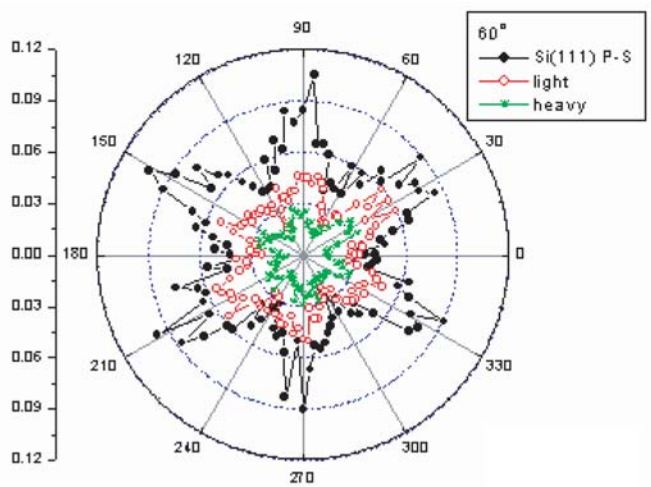


(b)

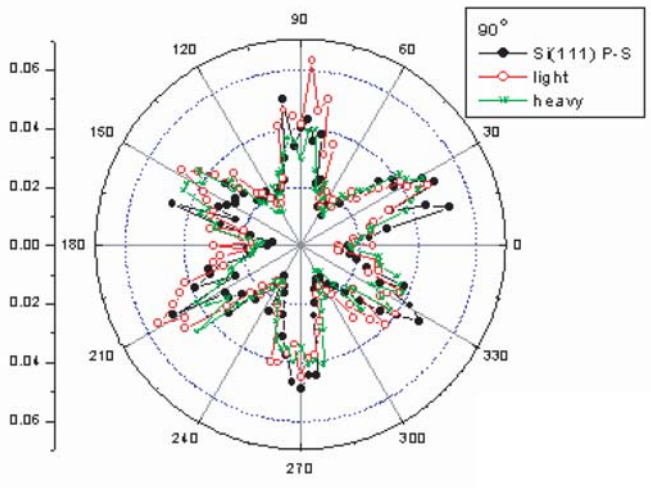


(c)

**Fig. 9.** The p-wave input and s-wave output SHG for Si(111) with various imposed forces and incident azimuthal angles.

in an asymmetric pattern for the surface scan of SH intensity. Considering the small response of the s-polarized SHG for isotropic silver metal, the threefold symmetric lobe is very prominent for granular silver films on a Si(111) surface. The symmetric surface SHG pattern induced by lattice-misfit strain can be illustrated by imposing an external force on a bare Si surface. The sensitive $\psi$-scan of surface SHG provides a clue to detecting the interface strain existing in multilayered films that cannot be elucidated by other surface analysis methods.

This work was supported from the National Science Council of the Republic of China under contract NSC94-2112-M007- and from the Ministry of Education under contract 92-FA-04-AA.

## References

1. W.L. Schaich, A. Liebsch, Phys. Rev. B **37**, 6187 (1988)
2. M. Weber, A. Liebsch, Phys. Rev. B **35**, 7411 (1987)
3. A. Liebsch, Phys. Rev. Lett. **61**, 1233 (1988)
4. R. Murphy, M. Yeganeh, K.J. Song, E.W. Plummer, Phys. Rev. Lett. **63**, 318 (1989)
5. J. Rudnick, E.A. Stern, Phys. Rev. B **4**, 4274 (1971)
6. A. Chizmeshya, E. Zaremba, Phys. Rev. B **37**, 2805 (1988)
7. C.S. Chang, J.T. Lue, Surf. Sci. **393**, 231 (1997)
8. J.E. Sipe, D.J. Moss, H.M. van Driel, Phys. Rev. B **35**, 1129 (1987)
9. T.F. Heinz, "*Nonlinear Surface Electromagnetic Phenomena*", edited by H.E. Ponath, G.I. Stegeman (Elsevier, Amsterdam, 1991), p. 353
10. C.C. Tzeng, J.T. Lue, Surf. Sci. **216**, 579 (1989)¡
11. C.C. Tzeng, J.T. Lue, Phys. Rev. A **39**, 191 (1989)
12. J.T. Lue, K.Y. Lo, C.C. Tzeng, IEEE J. Quantum Electron. **38**, 302 (1992)
13. J.T. Lue, C. Dai, Phys. Rev. B **47**, 13653 (1993)
14. C.S. Chen, J.T. Lue, C.L. Wu, S.G. Gwo, K.Y. Lo, J. Phys.: Condens. Matter **15**, 6537 (2003)
15. C.W. van Hasselt, M.A. Verheijen, Th. Rasing, Phys. Rev. B **42**, 9263 (1990)
16. J.Y. Huang, Jpn. J. Appl. Phys. **33**, 3878 (1994)
17. F.R. Aussenegg, A. Leitner, H. Gold, Appl. Phys. A **60**, 95 (1995)
18. I.L. Lyubchanskii, N.N. Dadoenkova, M.I. Lyubchanskii, Th. Rasing, Jae-W. Jeong, S.C. Shin, Appl. Phys. Lett. **76**, 1848 (2000)
19. S.V. Govorkov, V.I. Emel'yanov, N.I. Koroteev, G.I. Petrov, I.L. Shumay, V.V. Yakolev, J. Opt. Soc. Am. B **6**, 1117 (1989)
20. K.Y. Lo, J.T. Lue, Phys. Rev. B **51**, 2467 (1995)
21. A.M. Malvezzi, M. Allione, M. Patrini, A. Stella, P. Cheyssac, R. Kofman, Phys. Rev. Lett. **89**, 087401 (2002)